JOC Article

Photolysis and Oxidation of Azidophenyl-Substituted Radicals: Delocalization in Heteroatom-Based Radicals

Paul R. Serwinski,[†] Burak Esat,[‡] Paul M. Lahti,* Yi Liao,[§] Richard Walton,[||] and Jiang Lan[⊥]

Department of Chemistry, University of Massachusetts, Amherst, Massachusetts 01003
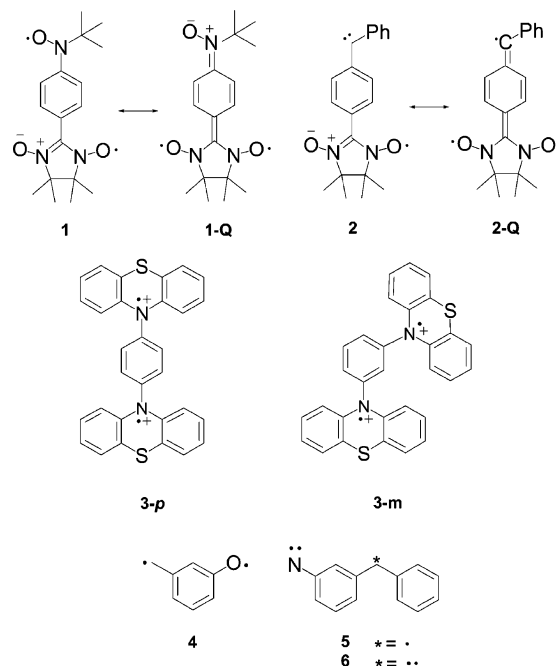
lahti@chem.umass.edu

Received March 26, 2004

2-(4-Azidophenyl)-4,4,5,5-tetramethyl-4,5-dihydro-1*H*-imidazole-3-oxide-1-oxyl (**14**), 2-(4-azidophenyl)benzimidazole-1-oxide-3-oxyl (**16**), 2-(4-azidophenyl)-1,2,6-triphenylverdazyl (**19**), 2-(3-azidophenyl)-4,4,5,5-tetramethyl-4,5-dihydro-*1H*-imidazole-3-oxide-1-oxyl (**21**), and (3-azidophenyl)-*N-tert*-butyl-*N*-aminoxyl (**25**) were photolyzed in frozen solution to give $S = 3/2$ state ESR spectra of the corresponding nitrenophenyl radicals with the following zero-field splitting parameters: $|D/hc| = 0.277$ cm^{-1}, $|E/hc| \leq 0.002$ cm^{-1} (**7** from **14**); $|D/hc| = 0.256$ cm^{-1}, $|E/hc| \leq 0.002$ cm^{-1} (**8** from **16**); $|D/hc| = 0.288$ cm^{-1}, $|E/hc| \leq 0.002$ cm^{-1} (**9** from **19**); $|D/hc| = 0.352$ cm^{-1}, $|E/hc| = 0.006$ cm^{-1} (**10** from **21**); $|D/hc| = 0.336$ cm^{-1}, $|E/hc| = 0.004$ cm^{-1} (**11** from **25**). UB3LYP/6-31G* computations and ESR spectroscopic analyses suggest that these are nitreno radicals, even para-linked systems with possible quinonoidal resonance forms. Neat samples of azidophenyl radicals **14** and **21** showed bulk paramagnetic behavior, consistent with the lack of close contacts in their crystal structures. Efforts to make photolabile coordination complexes of **14** and **21** with paramagnetic transition metal ions were unsuccessful: Cu(ClO4)$_2$·6H$_2$O instead oxidized them to the corresponding diamagnetic nitrosonium perchlorate salts.

Introduction

Various parity-based models are used to predict ground-state spin multiplicities of non-Kekulé systems, based upon molecular connectivity.[1] While these have been very successful, expectations can be confounded by molecular torsion or substituent effects.[2] Also, heteroatoms polarize spin density distributions in a π-system, so the best structural description may be unclear to casual inspec-

tion. For example, in **1**[3] and **2**,[4] both quinonoidal and

benzenoid structures are plausible. Experimentally, **1** does not exhibit major quinonoidal character in its crystal

† Present address: Sensor Research and Development Corp, Farmington, CT 06034.

‡ Present address: Gemsan A.S., Istanbul, Turkey.

§ Present address: Department of Chemistry, University of Washington, Seattle, WA 98195.

|| Present address: Ethox Chemicals LLC, Greenville, SC 29605.

⊥ Present address: Verizon Data Service, LAOMS62, 40 Sylvan Rd, Waltham, MA 02451.

(1) (a) Longuet-Higgins, H. C. *J. Chem. Phys.* **1950**, *18*, 265, 275, 283. (b) Longuet-Higgins, H. C. In *Theoretical Organic Chemistry, Kekulé Symposium*; Butterworth: London, 1958; p 9. (c) Ovchinnikov, A. A. *Theor. Chim. Acta* **1978**, *47*, 297. (d) Klein, D. J.; Nelin, C. J.; Alexander, S.; Matsen, F. E. *J. Chem. Phys.* **1982**, *77*, 3101. (e) Klein, D. J. *Pure Appl. Chem.* **1983**, *55*, 299. (f) Klein, D. J.; Alexander, S. A. In *Graph Theory and Topology in Chemistry*; King, R. B., Rouvray, D. H., Eds.; Elsevier: Amsterdam, The Netherlands, 1987; Vol. 51, p 404. (g) Borden, W. T.; Davidson, E. R. *J. Am. Chem. Soc.* **1977**, *99*, 4587. (h) Shen, M.; Sinanoglu, O. In *Graph Theory and Topology in Chemistry*; King, R. B., Rouvay, D. H., Eds.; Elsevier: Amsterdam, The Netherlands, 1987; Vol. 51, p 373.

(2) (a) Dvolaitzky, M.; Chiarelli, R.; Rassat, A. *Angew. Chem., Int. Ed. Engl.* **1992**, *31*, 180. (b) Kanno, F.; Inoue, K.; Koga, N.; Iwamura, H. *J. Am. Chem. Soc.* **1993**, *115*, 847. (c) Borden, W. T.; Iwamura, H.; Berson, J. A. *Acc. Chem. Res.* **1994**, *27*, 109. (d) Shultz, D. A.; Bodnar, S. H.; Lee, H.; Kampf, J. W.; Incarvito, C. D.; Rheingold, A. L. *J. Am. Chem. Soc.* **2002**, *124*, 10054. (e) Shultz, D. A.; Fico, R. M., Jr.; Bodnar, S. H.; Kumar, R. K.; Vostrikova, K. E.; Kampf, J. W.; Boyle, P. D. *J. Am. Chem. Soc.* **2003**, *125*, 11761. (f) Shultz, D. A.; Fico, R. M., Jr.; Lee, H.; Kampf, J. W.; Kirschbaum, K.; Pinkerton, A. A.; Boyle, P. D. *J. Am. Chem. Soc.* **2003**, *125*, 15426.

(3) Inoue, K.; Iwamura, H. *Angew. Chem., Int. Ed. Engl.* **1995**, *34*, 927.

(4) Matsuda, K.; Iwamura, H. *Mol. Cryst. Liq. Cryst., Sect. A* **1997**, *306*, 89.

structure.[3] System **3** has a singlet ground state in meta-connectivity and a triplet in para-connectivity, opposite to typical behavior for phenylene-based systems.[5] System **4** has no Kekulé structures due to its meta-connectivity, but simple frontier orbital arguments suggested the possibility of a singlet ground state until experiment[6] and theory[7] showed it to have a triplet ground state. Heterospin meta-connected nitrene plus radical or carbene systems **5**−**6** also show high-spin state behavior.[8] The interplay between substituent electronegativity, molecular connectivity, and molecular conformation thus confuses prediction of molecular ground states.

In this paper, we report details of the spectral characterization of five heterospin systems in which a nitrene spin site is exchange-linked to a radical spin site. All were generated by frozen solution photolysis of the corresponding azidophenyl precursors. 2-(4-Nitrenophenyl)-4,4,5,5-tetramethyl-4,5-dihydro-1*H*-imidazole-3-oxide-1-oxyl, 2-(4-nitrenophenyl)benzimidazole-1-oxide-3-oxyl, and 2-(4-nitrenophenyl)-1,2,6-triphenylverdazyl−structures **7**−**9**, respectively−all have para-connectivities that allow direct conjugation between the nitrene and radical sites.
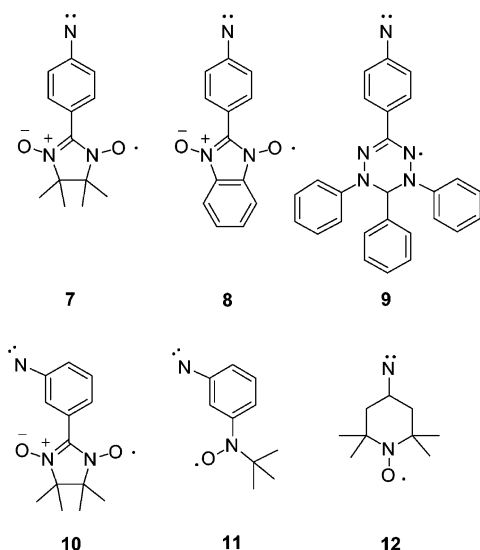
2-(3-Nitrenophenyl)-4,4,5,5-tetramethyl-4,5-dihydro-1*H*-imidazole-3-oxide-1-oxyl and 3-*N-tert*-butyl-*N*-aminoxylphenylnitrene−**10** and **11**, respectively−are meta-linked analogues that allow exchange, but not direct conjugative linkage between nitrene and radical sites. We have previously described some properties of **7**−**11**,[9] but to our knowledge only Wasserman has described[10] a related nitreno-radical system, **12**, which has no linking π-conjugative path. We also report magnetic measurements on the precursor radicals used to generate **7** and **10**, as well as the results of efforts to coordinate the precursor radicals with paramagnetic cations to make photolabile magnetic materials.[11] Details are given in the appropriate sections below.

Results

Synthesis and Characterization. The syntheses of the azidophenyl precursors to nitreneo-radicals **7**−**11** are shown schematically in Figures 1-2. Condensation of 4-azidobenzaldehyde with 2,3-bis(hydroxylamino)-2,3-dimethylbutane hydrogen sulfate[12] yielded bis-hydroxylamine **13**, which was oxidized with freshly made lead dioxide to deep blue radical **14**, which was fully characterized, including single crystal X-ray analysis (Supporting Information). It is relatively stable for months in the absence of direct light, but is best purified by column chromatography shortly before use.

Treatment of 4-azidobenzaldehyde with *o*-quinone bisoxime in acid yielded 2-(4-nitrenophenyl)benzimidazole-1-hydroxy-3-oxide, **15**,[13] which was difficult to dissolve in most solvents (presumably due to strong intermolecular hydrogen bonding) but could be oxidized to azido radical precursor **16** by dissolution in aqueous base and treatment with sodium periodate. Radical **16** appears to be stable for years in the absence of light.

4-Azidobenzaldehyde was converted[14] to **17**, and thence to hydroverdazyl **18**, which oxidized in situ to azidophenylverdazyl **19**, which was fully characterized including single-crystal X-ray analysis (Supporting Information). This dark green radical precursor can be stored for years without significant decomposition.

3-Azidobenzaldehyde was converted to the bis-hydroxylamine **20** and oxidized to give stable radical **21**, using the methodology described for the para-connected analogue (Figure 2). The radical was fully characterized, including two crystalline forms of **21** identified by X-ray analysis; a predominant orthorhombic $P2_12_12_1$ blue α-phase and a minor monoclinic $P2_1/c$ green β-phase (Supporting Information). Like its para-analogue **14**, **21** is best purified by chromatography just before use.

m-Dibromobenzene was metalated (Figure 2) and treated with 2-methylnitrosopropane followed by *tert*-butyldimethylsilyl chloride to give protected hydroxylamine **22**, which was again metalated and treated with tosyl azide to give **23**, deprotected to hydroxylamine **24**, and at once oxidized with lead dioxide to give reddish

(5) Okada, K.; Imakura, T.; Oda, M.; Murai, H.; Baumgarten, M. *J. Am. Chem. Soc.* **1996**, *118*, 3047.

(6) Rule, M.; Matlin, A. R.; Seeger, D. E.; Hilinski, E. F.; Dougherty, D. A.; Berson, J. A. *Tetrahedron* **1982**, *38*, 787.

(7) Horvat, D. A.; Murcko, M. A.; Lahti, P. M.; Borden, W. T*., J. Chem. Soc., Perkin 2,* **1998**, 1037.

(8) (a) Tukada, H. *Chem. Commun.* **1993**, 302. (b) Tukada, H.; Mutai, K.; Iwamura, H. *Chem. Commun.* **1987**, 1159. (c) Cf. also meta-linkage of phenylnitrene to a localized biradical to give a heterospin quintet system in: Tukada, H. *Org. Lett.* **2001**, *3*, 3261.

(9) (a) For **7**, a preliminary study was described in: Esat, B.; Walton, R.; Lahti, P. M. *J. Am. Chem. Soc.* **1998**, *120*, 5122. (b) Preliminary results for **8**−**11** were described in the proceedings of the VIIth International Conference on Molecular Magnetism: Lahti, P. M.; Esat, B.; Liao, Y.; Serwinski, P. R.; Lan, J.; Walton, R. *Polyhedron* **2001**, *20*, 1647. The ESR spectra for compounds **11** and **12** were inadvertently reverse labeled in that article: the zfs parameters were given correctly.

(10) Wasserman, E. *Prog. Phys. Org. Chem.* **1971**, *8*, 319.

(11) For an example of photochemical activation of bis(pyridyl)carbenes to link paramagnetic cations, see: (a) Koga, N.; Ishimaru, Y.; Iwamura, H. *Angew. Chem., Int. Ed. Engl.* **1996**, *35*, 755. (b) Sano, Y.; Tanaka, M.; Koga, N.; Matsuda, K.; Iwamura, H.; Rabu, P.; Drillon, M. *J. Am. Chem. Soc.* **1997**, *119*, 8246.

(12) (a) Ovcharenko, V.; Fokin, S.; Rey, P. *Mol. Cryst. Liq. Cryst. Sect. A* **1999**, *334*, 109. (b) Esat, B. Ph.D. Dissertation, University of Massachusetts, Amherst, MA, 2001.

(13) (a) Balaban A. T.; Halls P. J.; Katrizky A. R. *Chem. Ind.* **1968**, 651. (b) Boulton A. J.; Gripper-Gray A. C.; Katrizky A. R., *J. Chem. Soc. B* **1967**, 911. (c) Aurich H. G.; Weiss W. *Chem. Ber.* **1973**, 106, 2408. (d) Aurich H. G.; Stork K. *Chem. Ber.* **1975**, *108*, 2764. (e) Borah H. N.; Boruah R. C.; Sandhu J. S. *Heterocycles* **1985**, *23*, 1625.

(14) (a) Dormann, E.; Winter, H.; Dyakonow, W.; Gotschy, B.; Lang, A.; Naarmann, H.; Walker, N. *Ber. Bunsen-Ges. Phys. Chem.* **1992**, *96*, 922. (b) Kuhn, R., II; Trischmann, H. *Monatsh. Chem.* **1964**, *95*, 457−479.
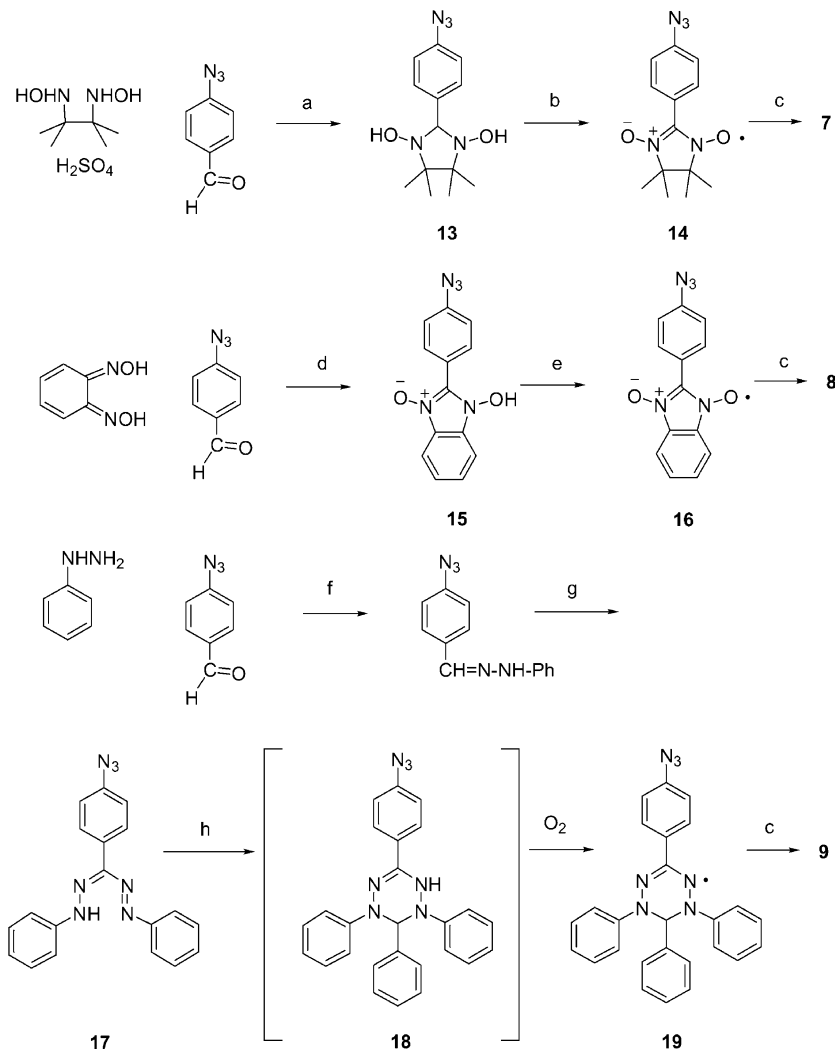
FIGURE 1. Synthesis of para-connectivity azido radical precursors: (a) MeOH/Et₃N, 25 h; (b) 0.25 M aq NaIO₄, CHCl₃; (c) 2-MeTHF, 77 K, *hν*; (d) EtOH, HBr, Δ, 48 h; (e) 0.25 M aq NaIO₄, CH₂Cl₂; (f) pyridine, 0 °C; (g) aniline/HCl/H₂O/NaNO₂; (h) NaOH/DMF/aq formaldehyde.

radical **25**. The radical is stable for months in the solid state if kept in the dark, but usually decomposes within 24 h in solution.

Photolysis and Spectroscopic Characterization. Frozen matrix UV–vis spectra were obtained in 2-methyltetrahydrofuran (MTHF) using a closed cycle circulating helium cryostat system. A blue frozen solution of **14** gave a magenta color that disappeared at once upon thawing to yield a greenish solution. Photolysis of yellow-green **16** gave a grayish-red matrix, which upon thawing yielded a straw yellow solution. Photolysis of green **19** gave deep purple matrix, which upon thawing yielded a brownish green solution. Photolyses of concentrated blue **21** and light orange **25** solutions under similar conditions gave rise to faint green-blue and tangerine orange colors, respectively, which disappeared upon thawing. Figures 3–7 show the observed spectral changes, which were much weaker for the meta than for the para-linked systems.

Electron spin resonance (ESR) spectra were obtained by 2–5 min photolysis of frozen, degassed MTHF solutions of **14**, **16**, **19**, **21**, and **25**, using a 1000 W xenon arc lamp (Pyrex filter or 350–500 nm band-pass filter).

Samples were placed into the cavity of an X-band spectrometer using a quartz LN2 finger dewar or rapidly transferred to a pre-cooled cavity (4.2–60 K, LHe cryostat). Alternatively, the frozen precursor samples could be photolyzed through a waveguide in the front of the spectrometer cavity, using a liquid light pipe guide.

The post-photolysis spectra are shown in Figures 8–12, along with plots of double-integrated spectral intensities of major peaks as functions of reciprocal temperature (Curie plots). Quartet-state zero-field splittings (zfs) were estimated using spectral line shape simulation[15,16] by the eigenfield method (Table 1). All quartet ESR features disappeared upon thawing of the matrixes, although excess reactant peaks in the *g* ∼ 2 region remained. Attempts to photolyze single crystals of **14** at 77 K gave no ESR signals other than a strong *g* ∼ 2 signal from the nitroxide group. If any nitreno radical is formed, it

(15) (a) Teki, Y. Ph.D. Dissertation, Osaka City University, Osaka, Japan, 1985. (b) Teki, Y.; Takui, T.; Yagi, H.; Itoh, K.; Iwamura, H. *J. Chem. Phys.* **1985**, *83*, 539.
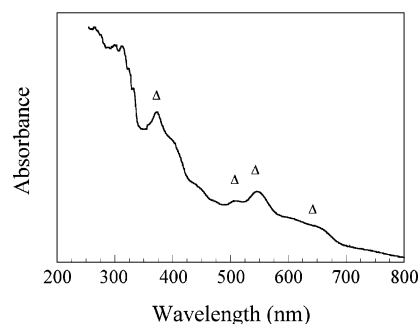(16) Sato, K. Ph.D. Dissertation, Osaka City University, Osaka, Japan 1994.
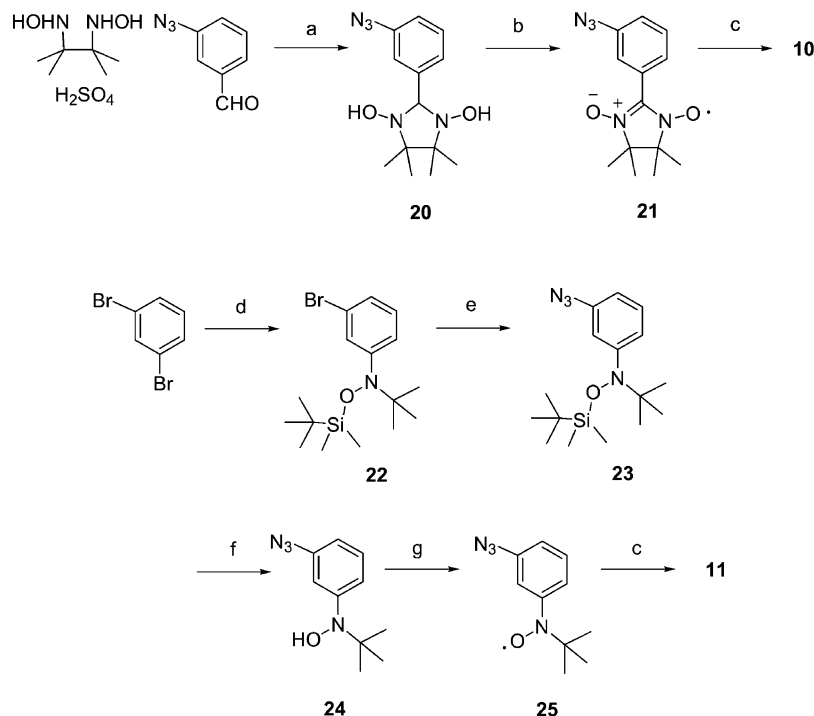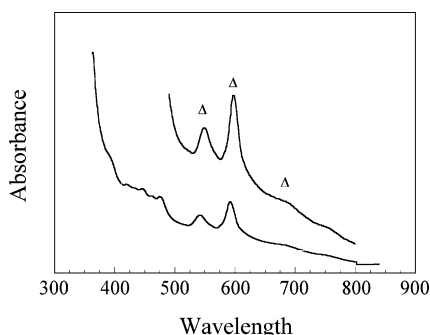
FIGURE 2. Synthesis of meta-connectivity azido radical precursors: (a) MeOH/Et₃N, 42 h; (b) 0.1 M aq NaIO₄, CH₂Cl₂; (c) 2-MeTHF, 77 K, *hν*; (d) BuLi, then Me₃CN=O, then ClSiMe₂CMe₃; (e) *n*-BuLi/Et₂O at −78 °C, warm to rt, add tosyl azide/Et₂O at −78 °C; (f) Bu₄NF, THF/CH₂Cl₂, 0 °C; (g) PbO₂, toluene.
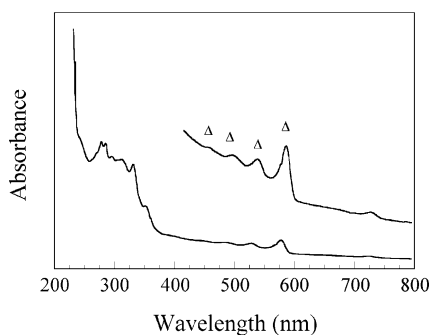
FIGURE 3. UV−vis spectrum from photolysis of **14** in frozen MTHF at 60 K, with triangles (△) showing peaks that are formed after photolysis at >300 nm.

FIGURE 4. UV−vis spectra from photolysis of **16** in frozen MTHF at 62 K, with triangles (△) showing peaks that are formed after photolysis at >300 nm.
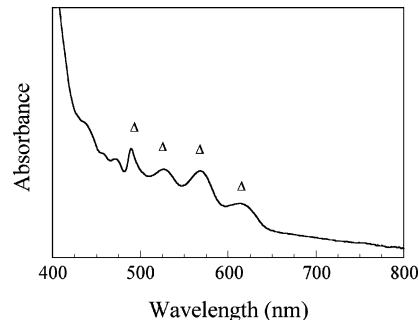

FIGURE 5. UV−vis spectra from photolysis of **19** in frozen MTHF at 60 K, with triangles (△) showing peaks that are formed after photolysis at >300 nm.

FIGURE 6. UV−vis spectra from photolysis of **21** in frozen MTHF at 60 K, with triangles (△) showing peaks that are formed after photolysis at >300 nm.

apparently reacts quickly with nearby radicals in the crystal lattice.

Magnetic Studies of the Nitronylnitroxides. Although the crystallographic data showed no close contacts

that suggested extended exchange interactions in the systems for which we could obtain crystallography, we tested the magnetic behavior of polycrystalline samples of **14** and **21** (which we were able to make in largest
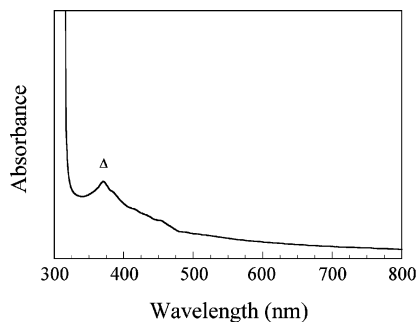
FIGURE 7. UV–vis spectra from photolysis of **25** in frozen MTHF at 60 K, with triangles (△) showing peaks that are formed after photolysis at >300 nm.

amounts) by dc magnetometry. Samples were placed in gelatin capsules and held in place with a small amount of cotton; before measurement, a helium purge procedure was carried out to avoid oxygen contamination. The magnetic susceptibility (χ) was analyzed at an external magnetic field of 1000 G over a temperature range of 1.8–300 K. Final measurements were corrected for temperature independent terms. Curie–Weiss fitting of the data for **14** gave a Curie constant of $C = 0.37$ emu-K/mol-Oe—indicating essentially 100% $S = 1/2$ spin carriers—and a moderate Weiss constant of $\theta = -2.6$ K. Nitronylnitroxide **21** also showed essentially paramagnetic behavior, with a Curie constant of $C = 0.37$ emu-K/mol-Oe and $\theta = -0.1$ K. Details are given in the Supporting Information. We did not study the magnetism of the azidophenyl radicals further.

Attempted Coordination Studies. We hoped to coordinate nitronylnitroxides **14** and **21** with M(hfac)$_2$ (M = Mn, Cu) to make linear chain polymers that could be photoactivated to allow extended exchange interactions in the solid state. Koga, Iwamura, and co-workers found such behavior in complexes of bis(pyridiyl)diazomethane complexes with paramagnetic ions.[11] Unfortunately, we failed to obtain characterizable radical complexes under any conditions that we attempted using M(hfac)$_2$-type paramagnetic ion sources.

26 X = N$_3$, Y = H
27 Y = N$_3$, X = H

14 X = N$_3$, Y = H
21 Y = N$_3$, X = H
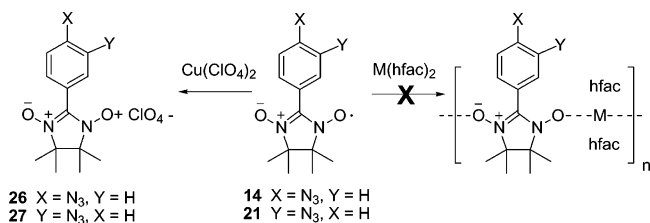
The only identifiable products were found in reaction of CuClO$_4$·6H$_2$O with **14** and **21** in CH$_2$Cl$_2$/EtOAc over 3 days to give deep-colored, crystalline solids that were insoluble in most organic solvents. The crystallographic analysis showed that Cu(II) ions were not incorporated, but rather that the nitroxyl radical fragments were oxidized to nitrosonium perchlorates **26** and **27**. The crystal structures of **26** and **27** showed significant shortening of the NO bonds relative to structures **14** and **21** (Table 2), consistent with loss of an electron from a singly occupied MO with antibonding N–O character. Magnetic susceptibility measurements of **26** and **27** showed no more than 2–3% of possible $S = 1/2$ spin units,
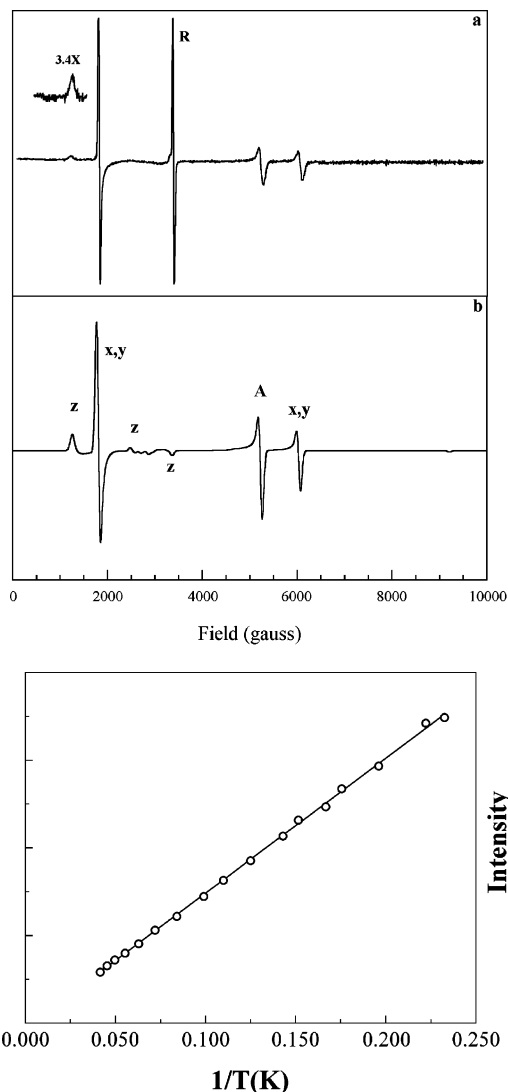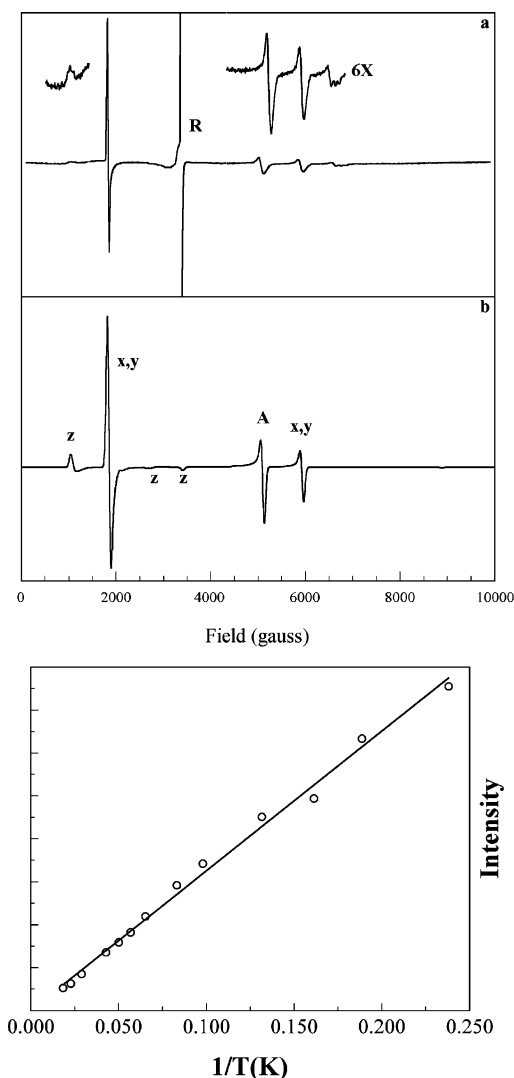

FIGURE 8. ESR spectrum from photolysis of **14** in frozen MTHF at 77 K after photolysis for 5 min with a Pyrex filtered xenon arc lamp (curve a), compared to eigenfield simulation (curve b) with the following parameters: $S = 3/2$, $g_{iso} = 2.003$, $|D/hc| = 0.277$ cm^{-1}, $|E/hc| = 0.000$ cm^{-1}, $\nu_0 = 9.557$ GHz. The label "R" shows the $g \sim 2$ remnant peak from the pre-photolysis reactant. Simulated peaks are assigned as x, y, z, and A = off-resonance transitions. The lower plot shows the intensity of the resonance at 1830 G as a function of reciprocal temperature (data) and the best linear fit to the data.

if all of the original NN units are considered as possible radical units. The residual susceptibility is presumably due to small amounts of unoxidized radical. Analogous nitrosonium salts with similar structures are unusual, but not unknown.[17] The conditions for forming **26** and **27** seem to be just right to allow oxidation of the radicals to the cations *and* subsequent rapid precipitation. Their oxidation capability and stability may make them useful cationic dopants. Further details are given in the Supporting Information. We did not carry out further investigations of these materials at this time.

(17) (a) Osiecki, J. H.; Ullman, E. F. *J. Am. Chem. Soc.*, **1968**, *90*, 1078. (b) Caneschi, A.; Laugier, J.; Rey, P. *J. Chem. Soc., Perkin Trans. 1* **1987**, 1077. (c) Caneschi, A., Gatteschi, D., Rey, P. *Prog. Inorg. Chem.* **1991**, *39*, 391.
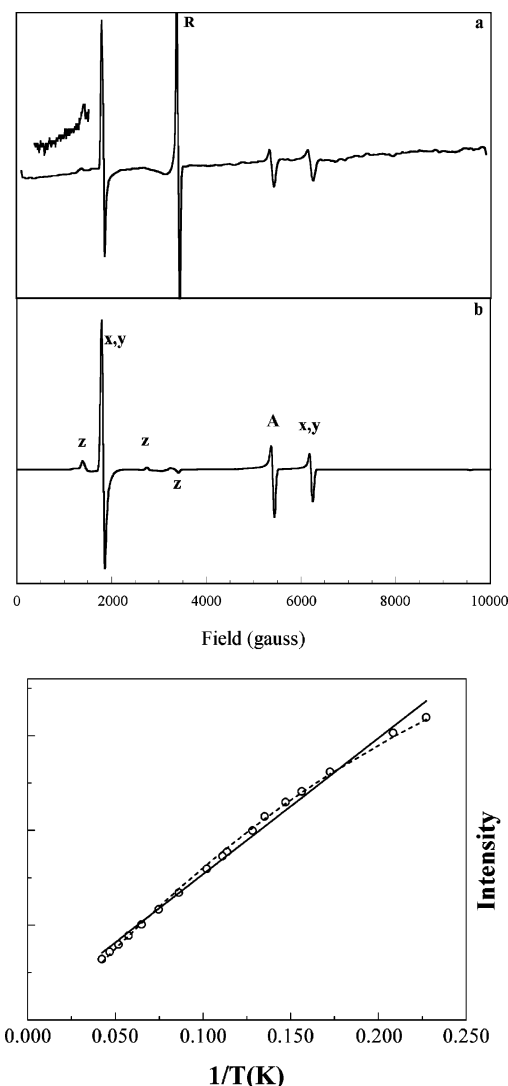
FIGURE 9. ESR spectrum from photolysis of **16** in frozen MTHF at 77 K after photolysis for 3 min with a Pyrex-filtered xenon arc lamp (curve a), compared to eigenfield simulation (curve b) with the following parameters: $S = 3/2$, $g_{iso} = 2.003$, $|D/hc| = 0.256$ cm^{-1}, $|E/hc| = 0.000$ cm^{-1}, $\nu_0 = 9.559$ GHz. The label "R" shows the $g \sim 2$ remnant peak from the pre-photolysis reactant. Simulated peaks are assigned as x, y, z, and A = off-resonance transitions. The lower plot shows the intensity of the resonance at 1840 G as a function of reciprocal temperature (data) and the best linear fit to the data.

Computational Studies. Computational studies were carried out on quartet and doublet states of model systems for **7**, **8**, **10**, and **11** using hybrid UB3LYP density functional theory (DFT) methodology[18] implemented in the program Gaussian 98[19] with a 6-31G* basis

(18) For DFT methodology used in this work, see: (a) Becke, A. D. *Phys. Rev. A* **1988**, *38*, 3098−3100. (b) Lee, C.; Yang, W.; Parr, R. G. *Phys. Rev. B* **1988**, *37*, 785.

(19) Frisch, M. J.; Trucks, G. W.; Schlegel, H. B.; Gill, P. M. W.; Johnson, B. G.; Robb, M. A.; Cheeseman, J. R.; Keith, T.; Petersson, G. A.; Montgomery, J. A.; Raghavachari, K.; Al-Laham, M. A.; Zakrzewski, V. G.; Ortiz, J. V.; Foresman, J. B.; Cioslowski, J.; Stefanov, B. B.; Nanayakkara, A.; Challacombe, M.; Peng, C. Y.; Ayala, P. Y.; Chen, W.; Wong, M. W.; Andres, J. L.; Replogle, E. S.; Gomperts, R.; Martin, R. L.; Fox, D. J.; Binkley, J. S.; Defrees, D. J.; Baker, J.; Stewart, J. P.; Head-Gordon, M.; Gonzalez, C.; Pople, J. A. Gaussian Inc.: Pittsburgh, PA, 1998.
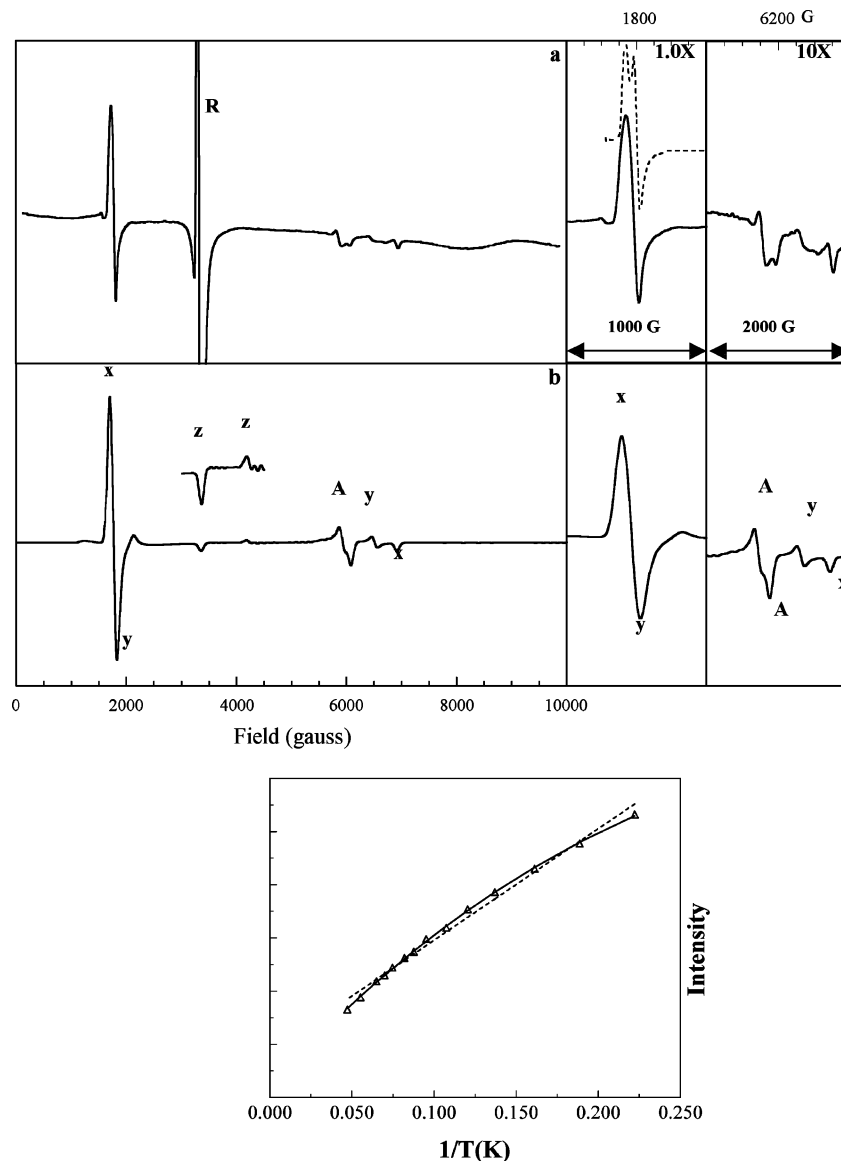
FIGURE 10. ESR spectrum from photolysis of **19** in frozen MTHF at 77 K after photolysis for 2 min with a Pyrex-filtered xenon arc lamp (curve a), compared to eigenfield simulation (curve b) with the following parameters: $S = 3/2$, $g_{iso} = 2.003$, $|D/hc| = 0.288$ cm^{-1}, $|E/hc| < 0.002$ cm^{-1}, $\nu_0 = 9.561$ GHz. The label "R" shows the $g \sim 2$ remnant peak from the pre-photolysis reactant. Simulated peaks are assigned as x, y, z, and A = off-resonance transitions. The lower plot shows the intensity of the resonance at 1830 G as a function of reciprocal temperature (data), the best linear fit to the data, and the best fit to eq 1 in the text.

TABLE 1. ESR Spectral Simulation Parameters for Quartet Species 7−11

quartet	simulation parameters
7	$S = 3/2$, $|D/hc| = 0.277$ cm^{-1}, $|E/hc| = 0.002$ cm^{-1}, $g_{iso} = 2.003$
8	$S = 3/2$, $|D/hc| = 0.256$ cm^{-1}, $|E/hc| < 0.002$ cm^{-1}, $g_{iso} = 2.003$
9	$S = 3/2$, $|D/hc| = 0.288$ cm^{-1}, $|E/hc| < 0.002$ cm^{-1}, $g_{iso} = 2.003$
10	$S = 3/2$, $|D/hc| = 0.352$ cm^{-1}, $|E/hc| = 0.006$ cm^{-1}, $g_{iso} = 2.003$
11	$S = 3/2$, $|D/hc| = 0.336$ cm^{-1}, $|E/hc| = 0.004$ cm^{-1}, $g_{iso} = 2.003$

set. Planar starting geometries were used, to consider the maximum possible conjugation effects. Summaries

FIGURE 11. ESR spectrum at 4.6 K from photolysis of **21** in frozen MTHF at 77 K for 7 min with a Pyrex-filtered xenon arc lamp (curve a), compared to eigenfield simulation (curve b) with the following parameters: $S = 3/2$, $g_{iso} = 2.003$, $|D/hc| = 0.352$ cm^{-1}, $|E/hc| = 0.006$ cm^{-1}, $\nu_0 = 9.372$ GHz. The label "R" shows the $g \sim 2$ remnant peak from the pre-photolysis reactant. Simulated peaks are assigned as x, y, z, and A = off-resonance transitions. Dashed line in the upper right expansion shows a 77 K spectral trace by comparison to the 4.6 K trace. The lower plot shows the intensity of the resonance at 1780 G as a function of reciprocal temperature (data), the best linear fit to the data, and the best fit to eq 1 in the text.

of UB3LYP/6-31G* //UB3LYP/6-31G* computed geometries and spin densities are given in the Supporting Information. Table 3 gives computed energies.

Discussion

Para-Connectivity Systems. A major purpose of this study was to evaluate the extent of spin density delocalization from the nitrene centers in para-linked systems **7**−**9** by comparison to meta-linked systems **10** and **11**. ESR is quite sensitive to unpaired electron spin distribution, so the spectral similarity of **7**−**9** suggests similar electronic natures. The spectra were well fit by quartet state simulations with a range of $|D/hc| = 0.256$−0.288 cm^{-1}. The lack of splitting in the major peaks at about

1800 G shows a near-zero value of $|E/hc|$, consistent with the pseudocylindrical structures in the para-connectivity.

Since the zfs in **7**−**9** is strongly affected by one-center nitreno nitrogen σ−π spin−spin interactions, increased delocalization of the nitrene π-spin will move spin density away from the localized σ-electron and decrease the zfs. Thus, the most delocalized nitrene is the benzimdazole-1-oxide-3-oxyl based system **8** (Table 1). But, assuming that $|D/hc|$ is directly proportional to the π-spin population on the nitrene nitrogen,[20] the experimental variation in nitrene π-spin is less than 10% among **7**−**9**. Computed

(20) (a) Coope, J. A. R.; Farmer, J. B.; Gardner, C. L.; McDowell, C. A *J. Chem. Phys.* **1965**, *42*, 54. (b) Ferrante, R. F. *J. Phys. Chem.* **1990**, *94*, 4, 3502. (c) The dependence of nitrene zfs upon spin density distribution has also been described by Wasseman in ref 10.
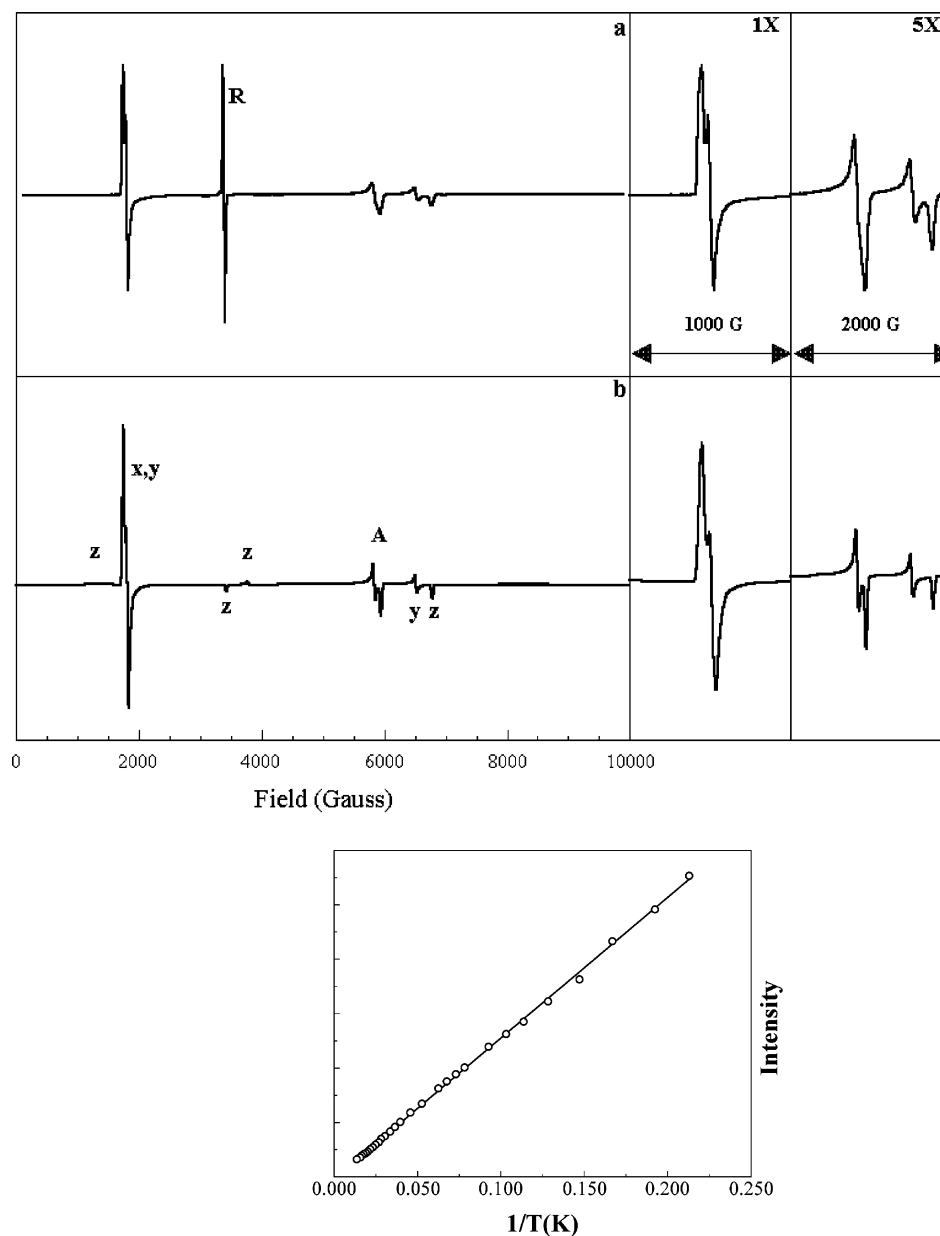
FIGURE 12. ESR spectra of **25** in frozen MTHF at 77 K after photolysis for 2 min with a Pyrex-filtered xenon arc lamp (curve a), compared to eigenfield simulation (curve b) with the following parameters: $S = 3/2$, $g_{iso} = 2.003$, $|D/hc| = 0.336$ cm^{-1}, $|E/hc| = 0.0045$ cm^{-1}, $v_0 = 9.560$ GHz. The label "R" shows the $g \sim 2$ remnant peak from the pre-photolysis reactant. Simulated peaks are assigned as x, y, z, and A = off-resonance transitions. The lower plot shows the intensity of the overlapping resonances at 1750−1800 G as a function of reciprocal temperature (data) and the best linear fit to the data.

Mulliken populations in **7**−**9** confirm this, showing a range of only 1.4−1.5 in the quartet state nitrene nitrogen spin populations (Supporting Information).

By comparison, the solution ESR spectra of the precursors to **7** and **8**—azido-radicals **14** and **16**—show a decrease in nitroxide hyperfine coupling from 7.4 to 4.5 G upon benzannelation. The experimental verdazyl nitrogen hyperfine coupling in **19** is intermediate at 5.4 G. The computed "nitroxide" nitrogen spin populations decrease from 0.40 to 0.22 in going from **7** to **9**, as spin density shifts from the nitroxide units onto the fused benzene ring. The radical nitrogens in the quartet state of **8** have spin populations of 0.22 and 0.46, similar to the ranges in **7**−**9**. Spin delocalization therefore varies

quite a bit within the radical moieties of the nitreno radicals. But, the limited computational variation of nitreno π-spin delocalization throughout the series **7**−**9** is the dominant factor that presumably yields the overall limited variation in experimental quartet state zfs.

Wasserman[11] described the splitting of a nitrene ESR xy-transition into two peaks by interaction with a nitroxide unit in **12** to give a pair of lines centered at 8300 G and split by 350 G. System **12** is not conjugated; hence, its nitrene-radical interactions depend on σ-bond spin polarization and through-space dipolar effects. The ESR spectra of **7**−**9** also exhibit two peaks in the high field region, but with larger splitting (820−830 G), reflecting
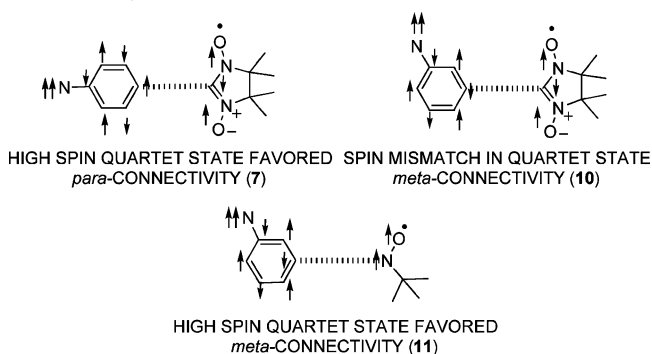
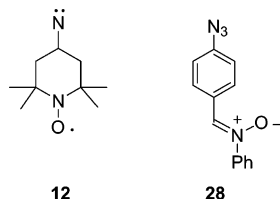**TABLE 2.   Comparison of Structural Parameters for Radicals 14, α-21, Nitrosonium Ions 26 and 27**

	14	α-21	26	27
rN−O	1.277(2)[a]	1.281(3)[a]	1.232(3)[a]	1.178(7)[a]
	1.286(2)	1.285(3)	1.234(3)	1.210(7)
rC−N (NN)[b]	1.356(2)	1.334(4)	1.335(4)	1.307(8)
	1.359(2)	1.343(4)	1.354(4)	1.331(7)
rNN−Ph[c]	1.455(3)	1.464(4)	1.459(4)	1.427(8)
rCC(aryl)	1.377(3)−1.397(3)	1.381(4)−1.392(5)	1.369(4)−1.400(4)	1.346(11)−1.378(8)
rC−N$_3$ (azide)	1.428(3)	1.431(5)	1.422(4)	1.402(9)
∠NN−Ph torsion[d] (deg)	23.0	31.7	49.0	29.5
∠NCCN torsion (NN)[e] (deg)	27.0	19.7	14.2	4.5
∠NCNO torsion (NN)[e] (deg)	1.8	0.2	1.1	1.2
	4.7	1.0	2.0	2.5
rNN····OClO$_3$	n/a	n/a	3.107(4)[f]	3.217(8)[f]
CCDC deposition no.	232910	232911	232914	232915

[a] Bond lengths in angstroms, angles in degrees, esd in parentheses. [b] NN = 4,4,5,5-tetramethyl-1-oxo-4,5-dihydroimidazolium-*N*(3)-oxide-2-yl moiety. [c] Interannular bond length. [d] Interannular torsion. [e] NN nonplanarity. [f] Closest perchlorate to nitrosonium approach. See the Supporting Information for more details.

SCHEME 1.   Spin Fragment Analysis of Nitreno Radical Systems

HIGH SPIN QUARTET STATE FAVORED
para-CONNECTIVITY (**7**)

SPIN MISMATCH IN QUARTET STATE
meta-CONNECTIVITY (**10**)

HIGH SPIN QUARTET STATE FAVORED
meta-CONNECTIVITY (**11**)

larger nitrene-radical interactions than in **12**, due to better interaction through π-conjugation.

12   **28**

We attempted to gauge delocalization of the nitrene onto a π-system similar to those in **7** and **8**. Photolysis of model compound **28** in frozen MTHF at 77 K with a Pyrex filtered 1000 W xenon arc lamp gave a strong at 6010 G, corresponding to a nitrene xy-transition with zfs of 0.66 cm^{-1}.[21] This nitrene peak is approximately in the middle of the region bracketed by the two high-field peaks of **7**−**9**, as expected for a phenylnitrene resonance split by the spin states of the connected radicals.

The para-connectivity nitreno radicals prefer high-spin computational ground states, consistent with their non-disjoint natures (Scheme 1). To test this experimentally, we measured ESR spectral peak intensities of the strongest quartet peaks in Figures 8−10 as functions of temperature (Curie plots). Systems **7** and **8** gave highly linear plots, and **9** showed very slight curvature. The former results are consistent either with substantial favoring of a high-spin ground state, or very nearly degenerate quartet and doublet states. If the observed slight curvature is not due to signal saturation, the Curie plot data for **9** corresponds to ΔE(D→Q) = 10−15 cal/mol using eq 1, where I/I_0 is the relative intensity of the major ESR spectral peak, T is the absolute temperature, and ΔE is the doublet to quartet energy gap when the doublet is the ground state. The computational results suggest that **7**-**9** have intrinsic high spin quartet ground states. The Curie plots for **7**-**8** are consistent with this. The Curie plot for **9** could correspond to either a very small preference for the low spin state, or to a high spin state with a slight amount of signal saturation despite our best efforts. The inherent uncertainties[22] of ESR Curie analysis do not allow a more definitive analysis of the data than this.

$$\frac{I}{I_0} = \frac{4e^{-\Delta E/RT}}{4e^{-\Delta E/RT} + 2} \qquad (1)$$

The balance of evidence suggests that **7**−**9** are nitreno radicals. The strong coloration of the intermediates (Figures 3−7) is reminiscent of quinone-like structures but could arise from charge-transfer-type excitations such as those described by Shultz.[23] Despite the variations in both computed (Supporting Information) and experimental spin density distributions within the nitronyl nitroxide, verdazyl, and benzimdazole-1-oxide-3-oxyl radical units, there is little variation in the computed nitrene spin delocalization or in the observed quartet zfs parameters that depend strongly on nitrene π-spin population. Overall, the computed spin density populations on phenylnitrene units of **7**−**9** seem inconsistent with a high degree of quinone-forming π-spin delocalization onto the various radical units, and the experimental ESR results support this argument.

Meta-Connectivity Systems. Systems **10** and **11** give ESR spectra that are quite different from the para-analogues. In both meta systems, the major peak at about 1800 G—as well as the higher field peaks—are split by a

(21) Ivonne Grajko synthesized compound **28** as an undergraduate research project. A 2-methyltetrahydrofuran solution of **28** was photolyzed with Pyrex-filtered light from a 1000 W xenon arc lamp at 77 K. A weak peak at about 6900 G (|D/*hc*| = 0.98 cm^{-1}) was attributed to a small amount of the nitrene in a twisted, nonconjugated conformation.

(22) The limitations of spectral Curie law analysis for determining ground-state spin multiplicity preference have been detailed, for example, by: Berson, J. A. In *The Chemistry of Quinoid Compounds*; Patai, S., Rappaport, Z., Eds.; John Wiley and Sons: 1988; Vol. 2, p 462.

(23) Shultz, D. A. *Polyhedron* **2003**, *22*, 2423.

TABLE 3.   UB3LYP/6-31G*//UB3LYP/6-31G*-Computed Energies for Model Nitreno Radicals[a]

Model Structure	UB3LYP/6-31G* Energies in Hartrees
	$E\,(^4A_1) = -662.259356 \;(\langle S^2 \rangle = 3.876)$ $E\,(^2A_1) = -662.249233 \;(\langle S^2 \rangle = 1.830); \Delta E = +6.3 \text{ kcal/mol}$
	$E\,(^4A_1) = -814.696377 \;(\langle S^2 \rangle = 3.868)$ $E\,(^2A_1) = -814.688684 \;(\langle S^2 \rangle = 1.814); \Delta E = +4.8 \text{ kcal/mol}$
	$E\,(^4A_1) = -583.2401014 \;(\langle S^2 \rangle = 3.845)$ $E\,(^2A_1) = -583.2339946 \;(\langle S^2 \rangle = 1.807); \Delta E = +3.8 \text{ kcal/mol}$
	$E\,(^4A') = -662.2502613 \;(\langle S^2 \rangle = 3.833)$ $E\,(^2A') = -662.2526367 \;(\langle S^2 \rangle = 1.897); \Delta E = -1.5 \text{ kcal/mol}$
	$E\,(^4A') = -455.5245965 \;(\langle S^2 \rangle = 3.822)$ $E\,(^2A') = -455.5185233 \;(\langle S^2 \rangle = 1.779); \Delta E = +3.8 \text{ kcal/mol}$

[a] All states optimized at the UB3LYP/6-31G* level of theory. Single multiplicity calculations done with broken symmetry and orbital mixing. $\langle S^2 \rangle$ shows computed spin squared expectation values for the state multiplicities shown. Methyl or pendant phenyl groups in the putative experimental species were replaced by hydrogens in the computations as shown.

non-zero zfs |E/*hc*| parameter (Table 1), consistent with a lower molecular symmetry. The spectrum for **10** shows thermally reversible line-narrowing at higher temperature, with better resolution of the splitting in the 1800 G peak at 77 K. We suspect this is due to changes in motion of the radical unit in **10** in the matrix, but we have no other direct evidence for this speculation.

Unlike the para-analogues, neither **10** nor **11** showed strong coloration; their UV−vis spectra exhibit shorter wavelength peaks, consistent with the lack of direct conjugation from nitrene to radical (Figures 6 and 7). The ESR zfs are substantially larger than those for the para systems. As mentioned above, the larger zfs indicates that the unpaired electrons are (on the average) closer together in the meta systems. This is consistent with the inability of the nitrene π-electron to delocalize directly onto the radical sites, which in turn leads to a larger nitrene nitrogen one-center $\sigma-\pi$ contribution. The computational results for **10** and **11** also show more spin density on the nitrene nitrogens than **7**−**9**. The best comparison is between connectivity isomers **7** and **10**; para-isomer **7** has a nitrene Mulliken spin density of 1.50, the meta-isomer **10** has 1.62. The observation of computed difference is consistent with the experimental larger zfs in the latter.

An interesting result is the theoretical spin density mismatch in the $^4A'$ state of **10**, at a transannular connection of β-spin density sites (Scheme 1 and Sup-

porting Information). Among the systems that we studied, only **10** can be formulated in this Borden−Davidson disjoint manner.[1g] System **10** is modeled to have a low-spin doublet ground state by about 1.5 kcal/mol (Table 3), unlike the computed high-spin quartet ground states of **7**−**9** and **11**. In an unconstrained UB3LYP/6-31G* computation, the interannular torsion was only 10.5° in **10**, so a low spin state seems unlikely to arise from torsional deconjugation alone.

By comparison, nitroxide-based **11** has a nondisjoint[1g] connection of the phenylnitrene to a large spin density nitroxide, favoring a high-spin ground state. The quartet-state UB3LYP/6-31G* spin density on the nitroxide nitrogen is 0.34, virtually identical to the value found for a simple phenyl methylnitroxide model system at the same level. Precursor **25** shows a strong, well-resolved ESR spectrum upon relatively brief photolysis, with no sign of a nitrene peak from conformationally twisted molecules. The UB3LYP computations show only a small torsion of the nitroxide relative to the phenylnitrene unit in the model system, <1°. AM1-UHF quartet state computations with the complete, *tert*-butyl nitroxide based system show only a 22° torsion of the N−O group relative to the phenyl ring. Substantial nitroxide torsion is known to be necessary to alter the high-spin preference of nondisjoint connectivities,[2] so a computed high-spin preference for **11** is reasonable.

System **10** shows a small curvature in its Curie law plot, consistent with a doublet to quartet energy gap of $\Delta E(\text{D}{\rightarrow}\text{Q})$ of not more than 13−15 cal/mol. This gap is quite small, similar to the most liberal estimate of a possible doublet state preference from the ESR Curie plot of nondisjoint system **9**. The likelihood of a low-spin ground state in **10** is thus based upon having both a slightly curved Curie plot and a computational low-spin state. By contrast, system **11** shows quite linear Curie law behavior, consistent with the computed high-spin quartet ground state (or an essentially degenerate high-spin with low-spin equilibrium). The nitroxide group should have the maximum delocalization onto the phenyl ring among the spin units used in **7**−**11**, so we feel that it should give rise to the strongest nondisjoint exchange interaction with the *m*-nitrene unit. As mentioned above, the limitations of Curie plot analysis make the experimental results nondefinitive, but the experimental results are consistent with the computational predictions for **10** and **11**.

Overall, the meta-connected systems cannot be formulated as quinonoidal molecules, but must by connectivity act as nitreno radicals. Systems **10** and **11** are disjoint and nondisjoint, respectively, and exhibit both Curie law behavior and computational spin state preferences that are consistent with these structural characterizations. Their larger zfs is consistent with qualitative expectations of lesser nitrene π-electron delocalization by comparison to the para-connected cases.

Conclusions

The systems in this study are tests of heteroatom substituent effects and of different types of spin-bearing units (heterospin systems) upon ground-state spin multiplicity and interelectronic exchange. We find that the ESR spectral zfs parameters do not vary greatly with the structure of the radical spin unit but are most affected by para- versus meta-connectivity. Since one-center interactions between σ- and π-spin populations on the nitreno nitrogen dominate the zfs, variations in the π-spin density distributions of the radical sites will not have so large an effect on quartet state zfs, consistent with the experimentally modest zfs variations in systems of the same connectivity. The smaller zfs in the para-connected set of molecules by comparison to the meta-connected set is consistent with greater π-electron delocalization from the nitrene site in the para systems. Still, all appear to have ESR spectral behaviors that are well-described as nitreno radicals, even when the radicals are para-conjugated to the nitrene site. It is not clear that it is proper to consider the para systems as having the maximum possible Kekulé-type bondedness, or to describe them as quinonoidal.

Neither the neat solid radicals, nor photolyzed neat radical samples, nor attempts at making photolabile coordination complexes with the radicals have yielded interesting bulk magnetic properties to date. Nevertheless, we hope that the molecular level information gained concerning the nature of delocalization of π-electron spin from the phenylnitrenes to the attached radicals will help with understanding exchange effects in other heterospin open-shell molecules, including related components of molecule-based electronic and magnetic materials.

Experimental Section

General Methods. 2,3-Bis(hydroxylamino)-2,3-dimethylbutane hydrogen sulfate was made by Ovcharenko's[24] method; 4-azidobenzaldehyde was obtained commercially (warning! possible explosion hazard under shock); 3-azidobenzaldehyde and tosyl azide were synthesized as described in the Supporting Information. 2-Methyltetrahydrofuran (MTHF) was distilled from calcium hydride before use.

2-(4-Azidophenyl)-1,3-dihydroxy-4,4,5,5-tetramethylimidazolidine (13). 2,3-Bis(hydroxylamino)-2,3-dimethylbutane hydrogen sulfate (0.499 g, 2.03 mmol) and 4-azidobenzaldehyde (0.328 g, 2.23 mmol) were dissolved in 15 mL of HPLC-grade methanol. To this mixture was added 0.209 g (2.06 mmol) of Et$_3$N. The mixture was stirred for 24 h under argon at room temperature and filtered. The resulting white solid was washed with 5 mL of ice-cold methanol and dried to give 0.135 g (24%) of white solid. Mp: 132−134 °C dec. ^{1}H NMR (DMSO-d_6): δ 7.77 (s, 2 H), 7.48 (d, 8.22 Hz, 2 H), 7.07 (d, 8.22 Hz, 2 H), 4.48 (s, 1 H), 1.05 (s, 6 H), 1.02 (s, 6 H). IR (KBr, cm^{-1}): 3450 (OH str), 3210 (CH str), 2945 (CH str), 2100 (N$_3$ stretch).

2-(4-Azidophenyl)-4,4,5,5-tetramethyl-4,5-dihydro-*1H*-imidazole-3-oxide-1-oxyl (14). To a suspension of 0.026 g (0.094 mmol) of **13** in 4 mL of chloroform was added 4 mL of 0.25 M aq NaIO$_4$ (1.00 mmol). A deep-blue color formed as soon as the oxidizing solution was added. The mixture was stirred at room temperature under argon for 5 min. The chloroform layer was separated, and the aqueous layer was extracted with 2 × 4 mL portions of chloroform. The combined organic layers were dried over anhydrous CaCl$_2$ and evaporated to yield 0.021 g (82%) of indigo-blue solid that was purified by silica gel column chromatography using 3:2 EtOAc/hexane as eluent to give a blue-black solid. Mp: 120−123 °C. Anal. Calcd for C$_{13}$H$_{16}$N$_5$O$_2$: C, 56.93; H, 5.84; N, 25.53. Found: C, 56.71; H, 5.97; N, 25.60. HR-MS (EI): calcd for C$_{13}$H$_{16}$N$_5$O$_2$ 274.1304, found 274.1304. ESR (9.781 GHz, CHCl$_3$): pentet, a_N = 7.4 G (2 N). UV−vis (CHCl$_3$, $\lambda_{max}(\epsilon)$, nm): 299 (15 400), 372 (5700), 625 (400). IR (KBr, cm^{-1}): 2945 (CH str), 2115 (N$_3$ str), 795

(24) Ovcharenko, V.; Fokin, S.; Rey, P. *Mol. Cryst. Liq. Cryst., Sect. A* **1999**, *334*, 109.

(*p*-phenylene); no OH band observed. Crystallography: deep blue prism, monoclinic $P2_1/c$ (No. 14) lattice; $a = 9.730(1)$ Å, $b = 9.960(1)$ Å, $c = 14.294(1)$ Å, $\beta = 101.36(1)°$, $V = 1358.07(10)$ Å^3, $Z = 4$, $D_{calc} = 1.342$ Mg/m^3; 1727 unique reflections with $I > 2\sigma(I)$ were modeled with 182 parameters to yield the structure with $R_1 = 0.0431$, w$R_2 = 0.1252$. See the Supporting Information for further details of the crystal analysis. This structure has been deposited at the Cambridge Crystallographic Databank Centre, CCDC deposition no. 232910.

Photolysis of 14 to 7. A MTHF solution of **14** was subjected to 3-fold freeze−pump−thaw degassing, frozen at 77 K, and photolyzed for 30−180 s with a 1000 W xenon arc lamp through a Pyrex filter. ESR (9.559 GHz, MTHF, 77 K): 1230 (wk), 1830 (s = strong), 3390 (s, remnant **14**), 5225, 6056 G. UV−vis (MTHF, λ_{max}, nm, 77 K): 320, 445 (wk), 486, 528, 578.

1-Hydroxy-2-(4-azidophenyl)benzimidazole-3-oxide (15). A mixture of 0.14 g (1.02 mmol) of *o*-benzoquinone-1,2-dioxime[13b] and 0.13 g (0.91 mmol) of 4-azidobenzaldehyde was stirred in 6 mL of absolute ethanol. Next, 0.69 g of 48% HBr was added to the mixture and the temperature increased to 33−35 °C. The blood-red mixture was stirred at this temperature under argon for 48 h with aluminum foil wrapping to avoid having direct light shine on the reaction. The solution was cooled to room temperature and 20 mL of distilled water added, which caused a precipitate. This solid was filtered and washed with 30 mL of distilled water and then with 30 mL of ethanol to yield a light beige solid. Neutralization of the filtrate with 5% aqueous sodium bicarbonate yielded a little precipitate, which was washed with water and ethanol and then combined with the first precipitate. The combined solids were dried under vacuum with minimum exposure to room light, to yield 0.09 g (38%) of product with that decomposes upon heating above 260 °C. IR (KBr, cm^{-1}): 3447 (OH str), 2119 (N$_3$ stretch). ^{1}H NMR(CDCl$_3$/CF$_3$COOH, MHz): δ8.08 (d, 2 H, $J = 8.84$ Hz), 7.76 (m, 2 H), 7.65 (m, 2 H), 7.27 (d, 2 H, $J = 8.84$ Hz).

2-(4-Azidophenyl)benzimidazole-3-oxide-1-oxyl (16). A mixture of 15 mg (0.057 mmol) of **15** and 2.2 mL of 0.1 M aqueous NaIO$_4$ was stirred for 15 min. Then, 5 mL of dichloromethane was added, followed by 2 mL of 5% aqueous NaHCO$_3$. The mixture was stirred for another 5 min. The pale green-yellow dichloromethane layer separated from the mixture, washed with aqueous saturated NH$_4$Cl, and dried over anhydrous MgSO$_4$. Evaporation of the solvent gave brownish solid product (6 mg, 40%, mp 138−141 °C). ESR (9.8 GHz): a_N(CHCl$_3$) = 4.51 G (2N), a_N(MTHF) = 4.39 G (2N), a_N(CCl4) = 4.18 G (2N). IR (CCl$_4$, cm^{-1}): 2120 (N$_3$ stretch). High-resolution MS-EI (*m/z*): 266.07 [266.0678 calculated for C$_{13}$H$_8$N$_5$O$_2$]. UV (MTHF, λ_{max}, nm): 250, 305, 315, 475.

Photolysis of 16 to 8. A MTHF solution of **16** was subjected to 3-fold freeze−pump−thaw degassing, frozen at 77 K, and photolyzed for 3 min with a 1000 W xenon arc lamp through a Pyrex filter. ESR (9.559 GHz, MTHF, 77 K): 1060 (wk), 1840 (s = strong), 3400 (s, remnant **16**), 5060, 5890, 6600 G (wk). UV−vis (MTHF, λ_{max}, nm 77 K): 320, 445 (wk), 486, 528, 578.

1-(4-Azidophenyl)-3,5-diphenylverdazyl (19). Phenyl hydrazine (1.0 mL, 10 mmol) was dissolved in 20 mL of pyridine at 0 °C, and 4-azidobenzaldehyde (1.3 mL, 1.59 g, 11 mmol) was added slowly to the reaction with stirring. The red solution was stirred at 0 °C for 1 h, following which 1 g of ice containing 1.0 mL of glacial acetic acid was added. The result was solution A, which contained the phenylhydrazone of 4-azidobenzaldehyde.

Aniline (1.0 mL, 1.0 g, 11 mmol) was dissolved in a solution made up of 1 mL of distilled water, 1 g of ice, and 2 mL of concd HCl and cooled to 0 °C. This solution was treated dropwise with a solution of 0.76 g (11 mmol) of sodium nitrite in 3 mL of water, keeping the reaction temperature at 0 °C. The result was solution B, which was stirred at 0 °C.

Solution B was added slowly dropwise to solution A, maintaining the reaction temperature at 0 °C for 1 h. The reaction was then heated to 60 °C for 15 min and then allowed

to cool to room temperature over 20 h. The reaction was filtered, and the brown solid was washed with a solution of 20 mL of methanol in 50 mL of water. The solid was air-dried to give formazan **17**, which was suitable for use in the next synthetic step.

Formazan **17** (0.47 g, 1.4 mmol) was placed in 20 mL of dimethylformamide and then treated with 0.16 g (0.5 mmol) of Ba(OH)$_2$· 8H$_2$O, followed by 2.9 g (19.0 mmol) of BaO. Next, 4.0 mL (5.75 g, 33.6 mmol) of benzyl bromide was added dropwise. The reaction was stirred at 0 °C for 2 h and then allowed to warm to room temperature for 1 h. The reaction was green at this point. The reaction was filtered, poured into 50 mL of toluene, and back-extracted with water. The organic layer could be evaporated to give a crude, dark green solid, which could be dissolved in methanol and allowed to cool in a refrigerator to yield green-black needles of verdazyl **19**. Mp: 146−148 °C. Anal. Calcd for C$_{26}$H$_{20}$N$_7$: C, 72.54; H, 4.68; N, 22.78. Found: C, 72.01; H, 4.83; N, 21.99. ESR (9.78 GHz, benzene): nonet, a_N = 5.4 G (4 N). UV−vis (MTHF, λ_{max}, nm): 290, 310, 320, 410, 442, 740 (broad). Crystallography: irregular green-black needle; monoclinic $P2_1/c$ (No. 14) lattice; $a = 6.5406(1)$ Å, $b = 13.1924(3)$ Å, $c = 6.5406(1)$ Å, $\beta = 95.0885(9)°$, $V = 2216.67(9)$ Å^3, $Z = 4$, $D_{calc} = 1.290$ Mg/m^3; 3559 unique reflections with $I > 2\sigma(I)$ were modeled with 380 parameters to yield the structure with $R_1 = 0.0761$, w$R_2 = 0.1731$. See the Supporting Information for further details of the crystal analysis. This structure has been deposited at the Cambridge Crystallographic Databank Centre, CCDC deposition no. 232913.

Photolysis of 19 to 9. A MTHF solution of **19** was subjected to 3-fold freeze−pump−thaw degassing, frozen at 77 K, and photolyzed for 2 min with a 1000 W xenon arc lamp through a Pyrex filter. ESR (9.561 GHz, MTHF, 77 K): 1380 (v wk), 1830 (s = strong), 3430 (s, remnant **19**), 5380, 6200 G. UV−vis (MTHF, λ_{max}, nm, 77 K): 300, 370, 400 (shoulder), 504, 553, 650 (broad).

2-(3-Azidophenyl)-1,3-dihydroxyl-4,4,5,5-tetramethyl-2H-imidazoline (20). A mixture of 1.01 g (4.08 mmol) of 2,3-bis(hydroxylamino)-2,3-dimethylbutane hydrogen sulfate and 1.01 g (6.78 mmol) of 3-azidobenzaldehyde (see the Supporting Information for synthesis) was stirred in 35 mL of methanol containing 2 mL of triethylamine under argon with protection from light for 42 h. The reaction was filtered, and the filtrate was evaporated completely to yield a yellow, viscous oil that was diluted with distilled water to give a solid. The solid was washed with distilled water dried in air with protection from direct room light to give 0.56 g (53%) of a slightly yellow solid. Mp: 140−143 °C. IR (KBr, cm^{-1}): 3410 (OH str), 3010 (CH str), 2910 (CH str), 2110 (N$_3$ stretch). ^{1}H NMR (CDCl$_3$) δ: 7.25 (s, 1 H), 7.1−7.3 (m, 2 H), 6.98 (m, 1H), 5.35 (br s, 2H), 4.68 (s, 1 H), 1.07 (s, 6 H), 1.06 (s, 6 H).

2-(3-Azidophenyl)-4,4,5,5-tetramethyl-2H-imidazoline-1-oxide-3-oxyl (21). To a 100 mL three-necked round-bottomed flask was added 0.113 g (0.409 mmol) of **20** and 15 mL of dichloromethane. The solution was stirred under argon while 15 mL of a 0.101 M sodium periodate solution was added. The reaction turned deep blue and was stirred for 5 min. The layers were separated, and the aqueous phase was extracted with 10 mL of dichloromethane. The organic layers were combined, washed with saturated ammonium chloride (3 × 10 mL), and dried over anhydrous magnesium sulfate. The solvent was evaporated, and the product was chromatographed on silica with a solvent system of 80/20 hexane/ethyl acetate (R_f = 0.14, dark blue). Yield: 0.065 g (58%) of azure crystals. Mp: 80−81 °C. Anal. Calcd for C$_{13}$H$_{16}$N$_5$O$_2$: C, 56.92; H, 5.58; N, 25.53. Found: C, 56.85; H, 5.86; N, 25.43. UV (CHCl$_3$, λ_{max}-(ϵ), nm,): 256 (11 000), 293 (3700), 366 (7600), 582 (308), 619 (280). IR (KBr, cm^{-1}): 3025 (sharp, arom C−H str), 2924 and 2850 (sharp, aliphatic C−H str), 2120 (N$_3$ stretch). MS (EI, *m/z*): 274.13 (C$_{13}$H$_{16}$N$_5$O$_2$ = M), 259.98 (M − 14), 246.12 (M − 28), 240.98 (M − 34). ESR (9.591 GHz, CH$_2$Cl$_2$): pentet, a_N = 7.48 G (2 N). Crystallography of α-phase: irregular deep

blue needles, orthorhombic $P2_12_12_1$ (No. 19) lattice; $a = 6.0831$-(2) Å, $b = 11.3917(5)$ Å, $c = 20.053(1)$ Å, $V = 1389.6(1)$ Å³, $Z = 4$, $D_{calc} = 1.311$ Mg/m³; 1107 unique reflections with $I > 2\sigma$-(I) were modeled with 181 parameters to yield the structure with $R_1 = 0.0349$, w$R_2 = 0.0942$. This structure has been deposited at the Cambridge Crystallographic Databank Centre, CCDC deposition no. 232911. Crystallography of β-phase: irregular green needles, monoclinic $P2_1/c$ (No. 14) lattice; $a = 7.3818(3)$ Å, $b = 17.5152(9)$ Å, $c = 12.1987(8)$ Å, $\beta = 120.0(18)°$, $V = 1407.07(13)$ Å³, $Z = 4$, $D_{calc} = 1.295$ Mg/m³; 1299 unique reflections with $I > 2\sigma(I)$ were modeled with 247 parameters to yield the structure with $R_1 = 0.0472$, w$R_2 = 0.1076$. See the Supporting Information for details of the crystal analyses. This structure has been deposited at the Cambridge Crystallographic Databank Centre, CCDC deposition no. 232912.

Photolysis of 21 to 10. A MTHF solution of **21** was subjected to 3-fold freeze−pump−thaw degassing, frozen at 77 K, and photolyzed for 7 min with a 1000 W xenon arc lamp through a Pyrex filter. ESR (9.371 GHz, MTHF, 4.6 K): 1550 (v wk), 1780 (strong), 3330 (strong, remnant **21**), 3750 5860, 6050 (min), 6510 (broad).

3-Bromo-*N*-*tert*-butyldimethylsiloxyl-*N*-*tert*-butylaminobenzene (22). This compound was prepared by our previously described procedure.[25]

3-Azido-*N*-*tert*-butyldimethylsiloxyl-*N*-*tert*-butylaminobenzene (23). To a solution of 1 g (2.8 mmol) of **22** in 20 mL of dry diethyl ether was added 1.85 mL (2.96 mmol) of a 1.6 N solution of *n*-butyllithium in hexane at −78 °C under argon. After being stirred for 45 min, the solution was warmed to room temperature for 30 min and then recooled to −78 °C for 30 min. A solution of 0.64 g (3.2 mmol) of tosyl azide (see the Supporting Information for synthesis) in 5 mL of dry diethyl ether was added, and the reaction was stirred in the dark under argon overnight at ambient temperature. The reaction was cooled to 0−5 °C and treated with a solution of 1.4 g (3 mmol) of sodium pyrophosphate decahydrate in 10 mL of water while maintaining the temperature. The reaction was then allowed to warm to room temperature and stirred in the dark under argon overnight. The resultant reaction mixture was diluted with 50 mL of diethyl ether and mixed. The organic layer was separated, dried over anhydrous magnesium sulfate, and evaporated under reduced pressure to give a brownish oil that was chromatographed on silica gel with hexane to give 0.74 g (83% yield) of product as a colorless oil. (All the workup steps were carried out in dim light.) This material was sufficiently pure to use in the subsequent step. ¹HNMR (CDCl₃, ppm): δ −0.12 (b, 6H), 0.91 (s, 9H), 1.1 (s, 9H), 6.76 (m, 1H), 6.97 (m, 2H), 7.19 (t, 1H, $J = 7.1$ Hz). FTIR (KBr, cm⁻¹): 2111 (N₃ stretch).

3-Azido-*N*-*tert*-butyl-*N*-hydroxylaminylbenzene (24). To a solution of 1.7 g (5.31 mmol) of **23** in 15 mL of dichloromethane was added 21 mL (21 mmol) of a 1 N solution of tetrabutylammonium fluoride in THF at 0 °C. The solution was stirred under argon overnight in the dark at room temperature. The solution was diluted with 30 mL of dichloromethane, 15 mL of water was added, and the reaction was stirred for 15 min. The organic layer was separated and dried over anhydrous magnesium sulfate. The organic solvent was evaporated under reduced pressure to give a brownish oil that was chromotographed on silica gel with 9:1 CH₂Cl₂/hexane. The result pinkish oil was kept in a freezer overnight to give a pinkish solid. The crude product was washed multiple times with hexane and finally with a bit of pentane to give 0.86 g of product (79% yield) as a white solid, mp 79−80 °C. All procedures were carried out with minimum lighting possible to limit sample photodecomposition. ¹HNMR (CDCl₃, ppm): δ 1.14 (s, 9H), 5.53 (s, 1H), 6.81 (m, 1H), 6.97 (m, 2H), 7.22 (t, 1H, $J = 7.1$ Hz). FTIR (KBr, cm⁻¹): 2110 (N₃ stretch). UV−

vis (toluene, λ_{max}, nm): 260 (shoulder), 290. Anal. Calcd for C₁₀H₁₄N₄O: C, 58.24; H, 6.84; N, 27.17. Found: C, 57.89; H, 6.79, N, 27.07.

Oxidation of 24 and Photolysis to 11. To a solution of 6 mg (0.029 mmol) of **24** in 6 mL of degassed toluene was added 10 mg (0.041 mmol) of recently prepared lead dioxide at room temperature. The reaction was stirred for 30 min in the dark, until TLC analysis of the solution showed no starting material left. The resulting orange-ish solution was separated from the lead dioxide, degassed, and used as is for ESR and UV spectroscopy. Radical **24** is fairly persistent in a diluted solution in the dark, but is not stable in a pure state even under argon in the dark below 0 °C. ESR (9.798 GHz, toluene, hfc derived by simulation with WINSIM[26]): $a_N = 11.9$ G (nitroxide nitrogen), $a_H = 2.00, 1.95, 1.80$ G. UV−vis (toluene, λ_{max}, nm): 268, 291, 391, 485.

A toluene solution of radical **24** was evaporated under vacuum, redissolved in MTHF, subjected to 3-fold freeze−pump−thaw degassing in a 5 mm o.d. quartz ESR tube, frozen to 77 K, photolyzed with a 1000 W xenon arc lamp for 5 min through a Pyrex filter, and analyzed by ESR spectroscopy. ESR (9.560 GHz, MTHF, 77 K): 1570 (wk), 1746 and 1804 (s = strong, overlapping), 3390 (s, remnant **24**), 3750 (v wk), 5837, 6525, 6765 G.

2-(4-Azidophenyl)-4,4,5,5-tetramethyl-1-oxo-4,5-dihydroimidazolium-*N*(3)-oxide Perchlorate (26). To a 50 mL Erlenmeyer flask was added 172 mg (0.63 mmol) of **14** and 264 mg (0.71 mmol) of copper(II) perchlorate hexahydrate. Next, 40 mL of 1:1 dichloromethane:ethyl acetate was added to the flask, which was then swirled vigorously. A black precipitate immediately formed. The reaction container was covered to prevent exposure to light. After 3 days, the supernatant liquid was purple. The vial was uncapped and allowed to evaporate slowly in the dark and then filtered, yielding purple-red crystals of **26** (81 mg, 34%, mp 152−153 °C). FTIR (KBr, cm⁻¹): 2924 (weak, aliphatic C−H str), 2121 (N₃ stretch). Anal. Calcd for C₁₃H₁₆ClN₅O₆: C, 41.78; H, 4.31; N, 18.74. Found; C, 41.54; H, 4.26; N, 18.71. CAUTION: Organic perchlorates are potential explosion hazards. Crystallography: deep red-purple needles, monoclinic $P2_1/c$ (No. 14) lattice; $a = 7.6357(2)$ Å, $b = 16.5403(5)$ Å, $c = 13.7750(5)$ Å, $\beta = 105.3791(12)°$, $V = 1677.44(9)$ Å³, $Z = 4$, $D_{calc} = 1.480$ Mg/m³; 2940 unique reflections with $I > 2\sigma(I)$ were modeled with 228 parameters to yield the structure with $R_1 = 0.0614$, w$R_2 = 0.1846$. This structure has been deposited at the Cambridge Crystallographic Databank Centre, CCDC deposition no. 232914.

2-(3-Azidophenyl)-4,4,5,5-tetramethyl-1-oxo-4,5-dihydroimidazolium-*N*(3)-oxide Perchlorate (27). To a 50 mL Erlenmeyer flask was added 173 mg (0.63 mmol) of **21** and 252 mg (0.68 mmol) of copper(II) perchlorate hexahydrate. Next, 40 mL of 1:1 dichloromethane/ethyl acetate was added to the flask, which was then swirled vigorously. The reaction container was covered to prevent exposure to light. After 1 day, the supernatant was greenish and a dark precipitate had formed. The reaction was filtered and the filtrate was allowed to evaporate slowly in the dark then filtered, yielding very dark red crystals of **27** (56 mg, 24%). Mp: 153−154 °C. FTIR (KBr, cm⁻¹): 2926 (weak, aliphatic C−H str), 2121 (sharp N₃ str). Anal. Calcd for C₁₃H₁₆ClN₅O₆: C, 41.78; H, 4.31; N, 18.74. Found: C 41.46, H 4.15, N 18.55. CAUTION: Organic perchlorates are potential explosion hazards. Crystallography: deep purple needles, monoclinic $P2_1/c$ (No. 14) lattice; $a = 7.2631(6)$ Å, $b = 13.4488(12)$ Å, $c = 16.958(2)$ Å, $\beta = 100.00$-(18)°, $V = 1610.3(3)$ Å³, $Z = 4$, $D_{calc} = 1.542$ Mg/m³; 2749 unique reflections with $I > 2\sigma(I)$ were modeled with 285 parameters to yield the structure with $R_1 = 0.0938$, w$R_2 = 0.2098$. This structure has been deposited at the Cambridge Crystallographic Databank Centre, CCDC deposition no. 232915.

ESR Spectral Studies. All ESR spectra were obtained using an X-band spectrometer, with samples consisting of 1−3

(25) Liao, Y.; Xie, C.; Lahti, P. M.; Weber, R. T.; Jiang, J.; Barr, D. P. *J. Org. Chem.* **1999**, *64*, 5176.

(26) Duling, D. R. *J. Magn. Reson.* **1994**, *B104*, 105.

mg of the appropriate azide precursor that was dissolved in about 500 μL of freshly distilled (from LiAlH$_4$) 2-methyltetrahydrofuran, placed in a stopcock-sealable 4 mm o.d. quartz tube, and subjected to 3-fold freeze−pump−thaw degassing. The sample was typically frozen at 77 K in a quartz finger Dewar with LN2, photolyzed for 1−5 min with a 1000 W xenon arc using Pyrex filtering, and then placed in the ESR cavity. Essentially the same results were observed when photolysis was done using a 350 nm band-pass filter, or 254 nm light from a Rayonet carousel photoreactor. For lower temperature studies, frozen, photolyzed samples were quickly transferred into a precooled ESR cavity (LHe cryostat at <60 K). Curie plots of ESR spectral intensities versus temperature were done by lowering the sample temperature to 4 K, checking the intensity of the doubly integrated main spectral peak as a function of the square root of applied microwave power, and running subsequent spectra in the upper portion of the power range where the 4 K signal intensity is still linear with square root of power (2 microwatts for this study).

Supporting Information Available: Experimental procedures not included in the main text; crystallographic information for **14**, **19**, and **21**; solution ESR spectra for **14**, **16**, **19**, **21**, and **25**; Gaussian summary information from UB3LYP/6-31G* computations on models for **7**−**9**, **11**, and **12**; plots of magnetic susceptibility for **14** and **19**; crystallographic information for nitrosonium salts **26** and **27**, field versus angular dependence plots for quartet spectral simulations. This material is available free of charge via the Internet at http://pubs.acs.org.

JO049500R